

Gain dependence on free carrier concentration in LGADs<sup>☆</sup>G. Kramberger<sup>a,\*</sup>, B. Hiti<sup>a</sup>, V. Cindro<sup>a</sup>, A. Howard<sup>a</sup>, I. Mandić<sup>a</sup>, M. Mikuž<sup>a,b</sup>, M. Petek<sup>a</sup>, A. Ristić<sup>c</sup>, G. Ristić<sup>c</sup><sup>a</sup> Jožef Stefan Institute, Jamova 39, SI 1000 Ljubljana, Slovenia<sup>b</sup> University of Ljubljana, Faculty of Mathematics and Physics, Jadranska 19, 1000 Ljubljana, Slovenia<sup>c</sup> University of Niš, Faculty of Electronic Engineering, Aleksandra Medvedeva 14, 18106 Niš, Serbia

## ARTICLE INFO

## Keywords:

Low Gain Avalanche Detectors  
Irradiations  
Time resolution  
Charge multiplication

## ABSTRACT

Low gain avalanche detectors (LGADs) were investigated with transient current technique utilizing 1064 nm light to determine the effect of ionization density on the measured gain. The ionization density was varied with laser intensity and width of the beam spot. A model was derived explaining the decrease of gain due to the polarization of the gain layer, which reduces the electric field. The model was also tested at different ionization densities for LGADs of different gain layer design.

## 1. Introduction

Low Gain Avalanche Detectors (LGAD) [1] are presently the technology of choice for track timing detectors in particle physics. A highly doped p<sup>+</sup> layer is implanted between the p-bulk and n-implant (n<sup>++</sup>-p<sup>+</sup>-p-p<sup>++</sup> structure) leading to a high enough electric field for impact ionization upon application of sufficient bias voltage (see Fig. 1a). Gain factors typically between 10 and 100 have been obtained. The use of thin LGADs (few tens μm) with high gain allows for superior timing resolution of these devices of several tens of ps [2]. The LGADs are also gaining interest in other applications such as single particle beam monitors [3], medical imaging (proton-CT) [4], X-ray imaging [5] etc. In these applications the ionization pattern is different from that of the minimum ionizing particle usually encountered in tracking applications. As shown in micro-beam tests using few MeV protons and ions the gain is almost completely lost [6,7]. On the other hand, studies of minimum ionizing electrons from a beta-source crossing detectors at even just a small angle already showed improvement in charge collection in comparison to perpendicular crossing [8]. Also, gain measured with Transient Current Technique showed a larger gain than that for beta-electrons, especially at large bias voltages [8].

The above observations can be explained by a ionization pattern of the different particles or light pulses, which leads to different ionization densities. This ranges from thousands e-h pairs/μm<sup>3</sup> for protons and ions to tens e-h pairs/μm<sup>3</sup> for minimum ionizing particles, assuming the ionization is typically contained within a lateral radius of ~ 1 μm as given by the Bethe-Bloch calculation. The lateral dimension of the generated e-h cloud increases due to multiple-scattering and diffusion

of the drifting charge, but even for low energy beta electrons in thin sensors it reaches typically only a few μm.

An external field separates the free carriers, but a large density of free carriers leads to a field screening effect after multiplication in the gain layer. That affects the impact ionization, and hence the gain of the LGADs. The gain of the LGADs thus becomes dependent not only on the gain layer design, applied voltage and temperature, but also on the particle that is being detected. It is the purpose of this paper to establish the relation between gain and density of ionization and propose a simple model that describes the observed data not only qualitatively but also quantitatively.

## 2. Samples and experimental technique

The LGAD and PIN (identical to LGAD, but without p<sup>+</sup> implantation) samples used in the study were produced by HPK.<sup>1</sup> The devices, PINs and LGADs, were single pads of size 1.3×1.3 mm<sup>2</sup> with active thickness of 50 μm. The low resistivity (≈ 0.01 Ωcm) Czochralski substrate was 150 μm thick and was metallized at the back.

Two different gain layer designs (implant depths and doping profiles) were used, HPK-T3.1 and HPK-T3.2, with gain layer depletion voltages  $V_{gl} = 41$  V and  $V_{gl} = 55.5$  V respectively. The exact gain layer design parameters are not revealed by the HPK, but HPK-T3.1 has shallower gain layer depth ( $x_{gl} \sim 1.5$  μm) than HPK-T3.2 ( $x_{gl} \sim 2$  μm) with similar implant widths and doping levels.

A device without an implanted gain layer was also used, HPK-PIN, which otherwise has all the same properties as the LGADs. The high resistivity epitaxial p-layer (active layer) is depleted at around 5 V,

<sup>☆</sup> Work performed in the framework of the CERN-RD50 collaboration.

\* Corresponding author.

E-mail address: [Gregor.Kramberger@ijs.si](mailto:Gregor.Kramberger@ijs.si) (G. Kramberger).

<sup>1</sup> Hamamatsu Photonics, Hamamatsu, Japan

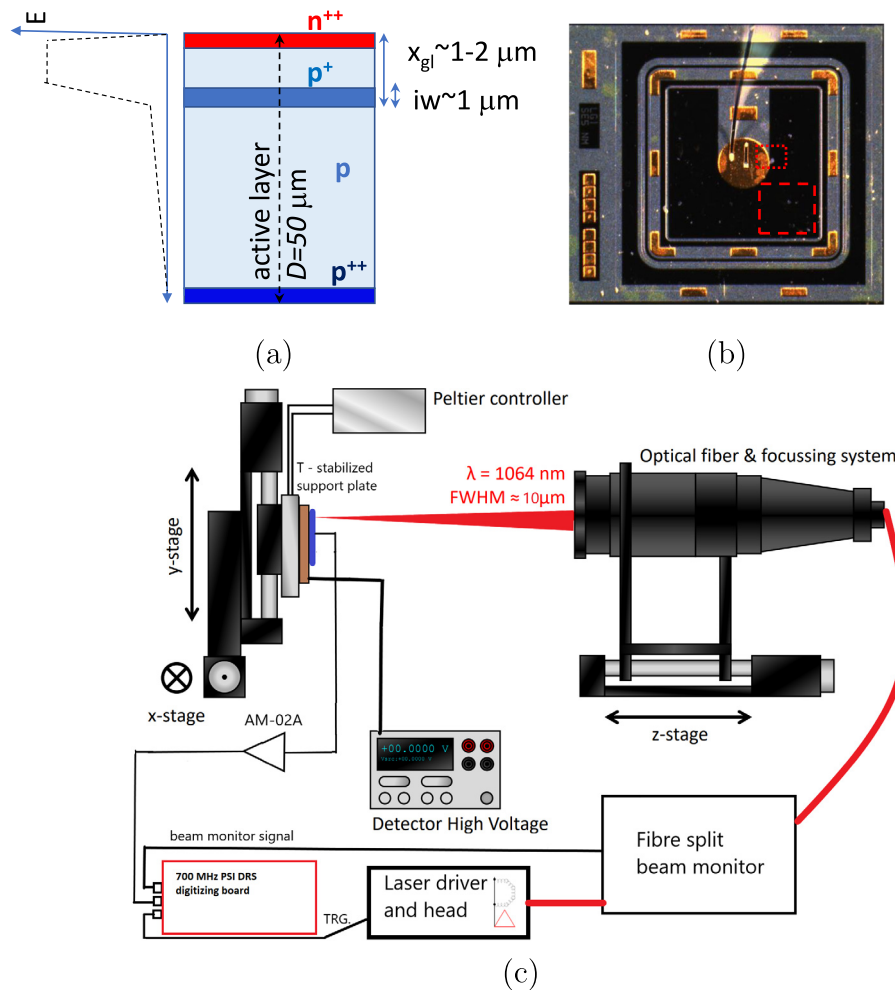


**Fig. 1.** (a) Schematic view of the LGAD (not to scale) indicating the most important design parameters: implant width ( $iw$ ), gain layer depth  $x_{gl}$ , and thickness  $D$ . Note that the implants ( $n^{++}$ ,  $p^+$ ) are not abrupt, that the low resistivity substrate at the back ( $p^{++}$ ) is not shown in its full thickness and that the figure is not to scale. (b) Photo of the device under study. The region used for determining the focus (dotted line) and used for screening studies (dashed line) is indicated. (c) Schematic view of the scanning transient current setup used in the studies.

resulting in the full depletion voltage of the LGAD of  $V_{fd} \sim V_{gl} + 5 \text{ V}$ . The front surface of the devices is mostly not metallized and are therefore suitable for studies with transient current technique using light pulses [9]. A photo of the device is shown in Fig. 1b.

The samples were studied with Particulars<sup>2</sup> scanning transient current technique system shown in Fig. 1c. Electron hole pairs (e-h) were generated in silicon by  $\sim 350 \text{ ps}$  (500 Hz repetition) wide pulses of infra-red light (1064 nm) with penetration depth of  $\sim 1 \text{ mm}$  at room temperature. The current induced by the motion of free carriers in the sensor is measured by a fast trans-impedance amplifier (3 GHz, 53 dB) and recorded by a fast digitizing circuit [10]. The full translation system with optics allows to focus the light to about  $\text{FWHM} \sim 10 \mu\text{m}$ . The system is equipped with a so called beam-monitor, where the beam is split into two beams of equal intensity. One branch is used for studying the sensor and the other is fed to a calibrated photo-diode. The latter is used to determine the absolute amount of charge injected in the tested sensor. All the tests were done at room temperature.

### 3. Measured results

The density of carriers is determined by laser power and spot size of the light pulse. This gives a unique possibility, which is not possible with particles, to control the density of carriers and test gain

dependence on free carrier concentration by using different ways of changing the ionization density. The relative intensity of the laser is well controlled, but the corresponding amount of carriers created in the silicon by the laser pulse is usually not precisely known. For the studies conducted in the paper knowing the absolute amount of charge is crucial.

#### 3.1. Calibration

In order to correlate the charge generated in the sensor with the one in the beam-monitor we used  $^{241}\text{Am}$   $\alpha$ -particle source. The emitted  $\alpha$  particles have energy of 5.486 MeV. Before hitting the sensor they have to travel through a gold foil covering the source, around 10 mm of air, and the surface oxide layer/passivation (non-active region) with effective thickness of around 1-2  $\mu\text{m}$ .<sup>3</sup> Taking this into account the deposited energy in the silicon would be around 4 MeV [11]. The response from  $\alpha$ -s was measured in a HPK-PIN detector as an average of 500 hits with a self-trigger level well below the measured induced current amplitudes. If accounted for the distribution of the angles under which the  $\alpha$ -s hit the sensor (longer path in the air and passivation), the average signal corresponds roughly to  $10^6$  e-h pairs.

An example of induced currents from  $\alpha$ -particle and IR laser in HPK-PIN sensor are shown in Fig. 2a, while the induced charge (integral of

<sup>2</sup> Particulars Ltd., Domžale, Slovenia

<sup>3</sup> Not revealed by the producer.

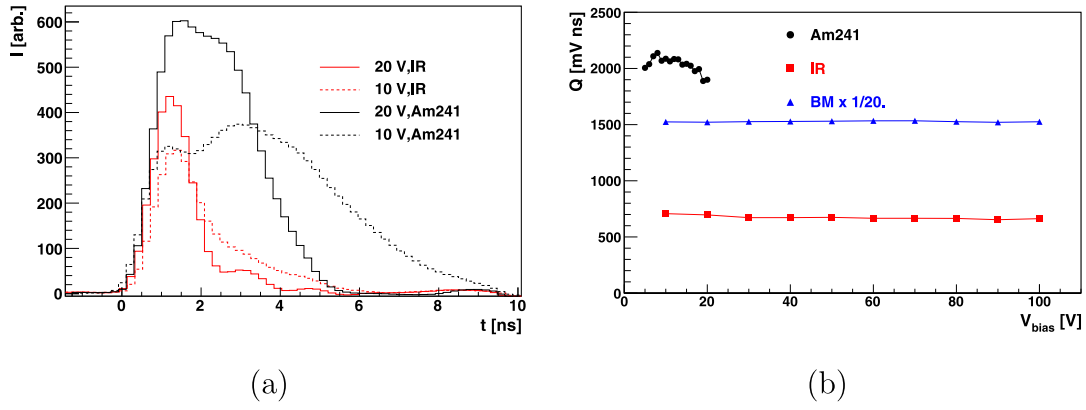


Fig. 2. (a) Induced current signals in the investigated HPK-PIN device after illumination with IR light pulses and  $\alpha$  particles from  $^{241}\text{Am}$  source. (b) Induced charge dependence on voltage for the currents shown in (a). The much longer pulse of the photo-diode used for absolute calibration of the laser pulse (Beam Monitor), not shown in (a), is scaled by 1/20.

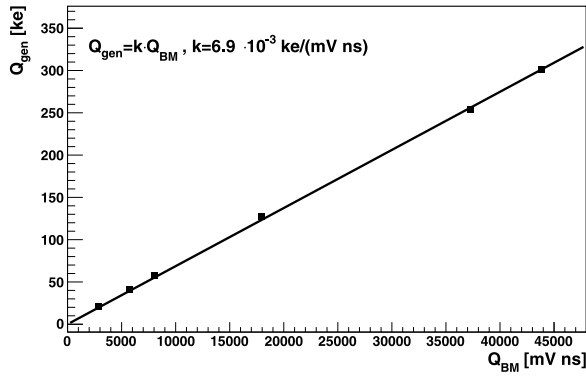


Fig. 3. The dependence of the charge generated in 50  $\mu\text{m}$  thick devices on beam-monitor signal. The fit of the linear function to the measured data is shown with a solid line.

current) dependence on bias voltage is shown in Fig. 2b. The beam monitor pulse is much longer due to slower electronics, and the charge  $Q_{BM}$  was obtained by the integration of the response in the time window of 140 ns. Although the ionization density of  $\alpha$  particles is much larger than that of minimum ionizing particles or laser pulses, there is no indication of recombination, which would show as dependence of  $Q_\alpha$  on bias voltage. The amplitude of the induced current was already close to saturation of the amplifier and the dynamic range of the digitizing board. Therefore it was not possible to accurately measure  $Q_\alpha$  at higher voltages than 20 V.

The generated charge  $Q_{gen}$  in the sensor is then calculated as

$$Q_{gen} \approx \frac{Q_{IR}}{Q_\alpha} \cdot 10^6 e_0, \quad (1)$$

where  $Q_{IR}$ ,  $Q_\alpha$  are the integrals of the induced currents over 30 ns window and  $e_0$  is the elementary charge. The charge generated by the laser pulse,  $Q_{gen}$ , can be determined from the beam monitor charge  $Q_{BM}$  providing that IR laser fully illuminates the detector surface and the optical settings (iris opening) are fixed. The relation between the  $Q_{gen}$  and  $Q_{BM}$  during our studies is shown in Fig. 3. The measurements of the beam-monitor signal can be therefore used to estimate the generated charge in the PIN diode. In order to verify the above calibration, IR laser signals in 300  $\mu\text{m}$  thick p-n diode were measured and as expected a six times larger  $Q_{IR}$  at the same  $Q_{BM}$  was obtained.

### 3.2. Focus search and determination of density of generated carriers

The density of generated carriers depends on the size of the laser beam spot on the detector surface. The focus of the beam is determined

by the knife edge scan over the metallized part of the detector surface (see inset of Fig. 4a). The dependence of the measured charge  $Q$  on position can be fit with the Error function (shown in Fig. 4a) from which the full width at half maximum (FWHM) for the beam was extracted.

The FWHM of the beam at different positions of the optical system with respect to the sensor's surface is shown in Fig. 4b. The minimum beam spot size is around 10  $\mu\text{m}$  and increases to  $\sim 100 \mu\text{m}$  by changing the position of the optical system by 1 mm (z-axis, see Fig. 1). The depth of focus of the beam is around 200  $\mu\text{m}$  long hence there is little change in beam width over the active thickness of the device. A large penetration depth of the IR light in silicon ( $> 1 \text{ mm}$ ) also assures uniform distribution of e-h pairs along the sensor depth. The measured data were fit with the equation describing the Gaussian beam shown with the extracted parameters in Fig. 4b.

The free carriers density  $n_{e-h}$  in the beam volume can be therefore approximately calculated as

$$n_{e-h} \approx \frac{Q_{gen}}{\pi R^2 D e_0}, \quad (2)$$

where  $R = \text{FWHM}/2$  and  $D$  is the thickness of the active layer. The concentration of electron-hole pairs can therefore be changed by the laser intensity ( $Q_{gen}$ ) or by changing the beam spot size ( $R$ ).

### 3.3. Gain measurements

The gain of the LGAD measured with infra-red light pulses was defined as  $G = Q_{IR}/Q_{gen}$ . The measurement of the gain dependence on bias voltage at a fixed laser intensity, but for different  $FWHM$ , is shown in Figs. 5 for both investigated samples. Also shown are measurements of gain with  $^{90}\text{Sr}$ , defined as  $G = Q_{Sr90}/Q_{PIN}$  [12]. A much lower gain than measured with laser is observed at high bias voltages, an effect of larger ionization density.

The suppression of the gain can be better seen when the charge normalized to charge at the largest  $R$  (i.e. smallest density) is plotted as a function of optical distance as shown in Figs. 6. There is no dependence of induced charge on  $R$  for HPK-PIN pointing on negligible free carrier recombination. This confirms that any change of induced charge for different  $R$  is related to the gain mechanism.

A sizable decrease of gain can be seen at small  $R$  for HPK-T3.2 (Fig. 6a). The decrease is larger at higher bias voltages. A much smaller gain for HPK-T3.1 was compensated by larger  $Q_{gen} = 77 \text{ ke}$  so that  $G \cdot Q_{gen}$  was similar as for HPK-T3.2 at  $Q_{gen} = 13 \text{ ke}$  (see Figs. 5). However, smaller decrease of gain of only few percent with  $R$  was observed for HPK-T3.1 (see Fig. 6b). This shows that the reduction of the field due to screening affects the operation at higher gain more.

Due to the limited range of the digitization board, it was not possible to cover the whole bias voltage range for all laser settings for HPK-T3.1

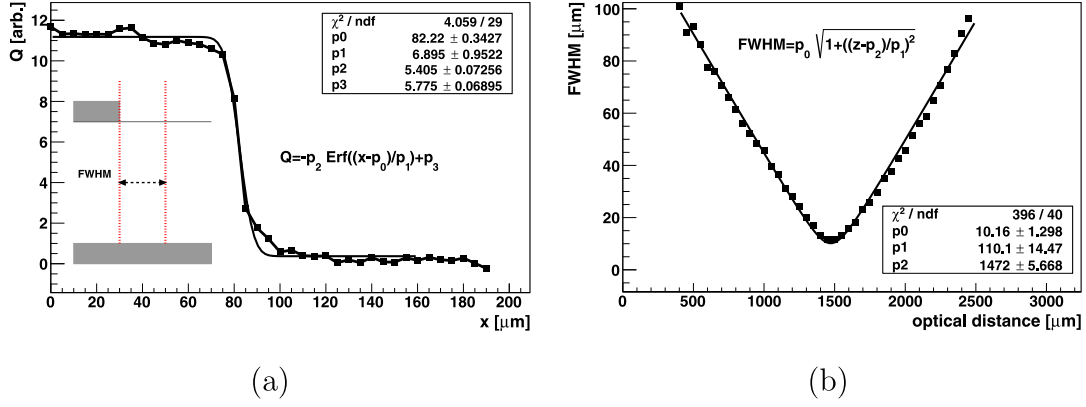


Fig. 4. (a) The example of focus determination in the investigated devices. (b) Dependence of beam width on distance of the sensors from the optical system.

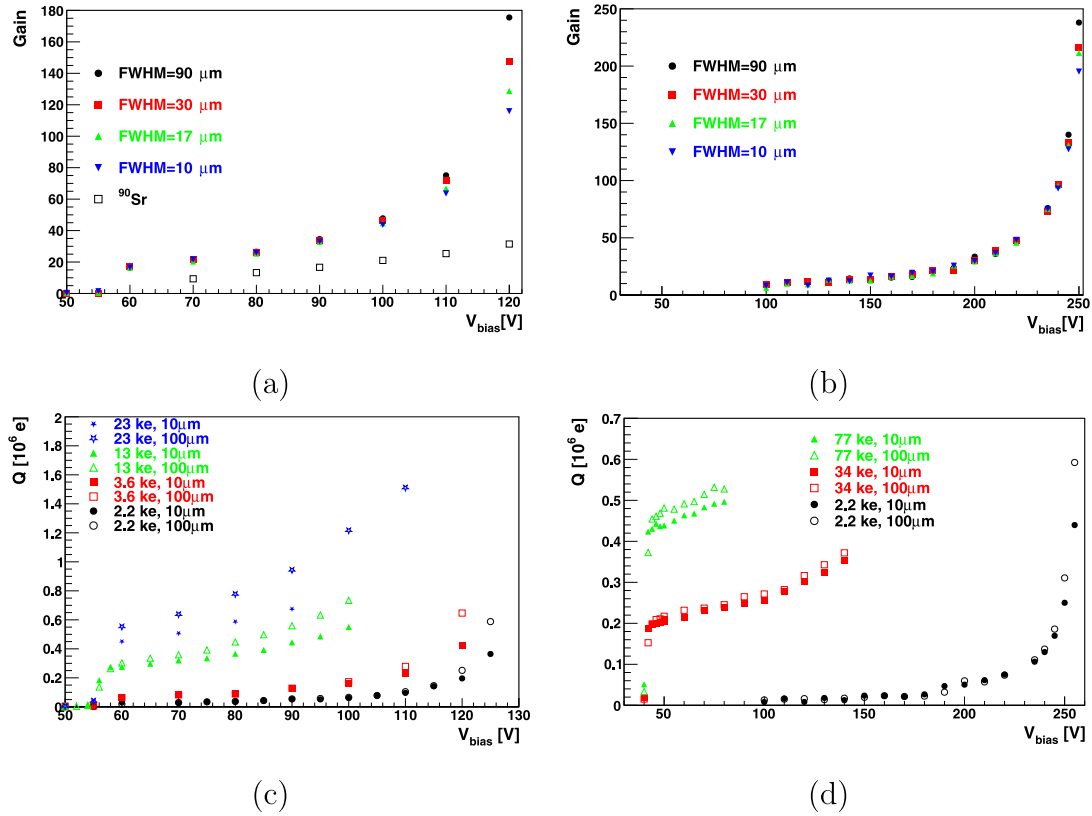


Fig. 5. The dependence of gain on bias voltage for different beam spot sizes: (a) HPK-T3.2 at  $Q_{gen} = 3.6$  ke, (b) HPK-T3.1 at  $Q_{gen} = 2.2$  ke. Collected charge dependence on voltage for different  $Q_{gen}$  and minimum and maximum beam spots: (c) HPK-T3.2 and (d) HPK-T3.1. The most probable signal of a  $^{90}\text{Sr}$  electron is  $\sim 3.4$  ke.

(see Fig. 5d). At the lowest laser intensity the difference appeared only at voltages above 230 V, while at high laser intensity the gain difference becomes apparent immediately after full depletion of the device, but the reachable gain is limited.

### 3.4. Modeling of the screening

The reduction of gain is a consequence of the reduced electric field in the presence of a large concentration of the carriers in the gain layer. The concentration of multiplied holes increases with depth and reaches its maximum at the end of the gain layer. On the other hand the concentration of electrons increases and reaches the maximum at the beginning of the gain layer. As the impact ionization in the gain layer produces an equal number of electrons and holes the difference in their concentration at both ends of the gain layer leads to a rise of

an electric field which opposes the external field due to applied bias voltage. The doping concentration of the gain layer implant is usually  $10^{15} - 10^{17} \text{ cm}^{-3}$ , hence the free carrier density due to a particle/laser pulse, which are or the order  $< 10^{14} \text{ cm}^{-3}$ , is only a perturbation to the space charge.

The electric field due to polarization of the gain layer ( $E_{int}$ ) can be approximated by assuming parallel plate capacitor, where the multiplied charge  $((G-1) \cdot Q_{gen})$  in the gain layer is assumed to be projected on the electrodes

$$E_{int} = \frac{Q_{gl}}{x_{gl} C_{gl}}, \quad Q_{gl} = (G-1) e_0 n_{e-h} x_{gl} S, \quad C_{gl} = \epsilon \epsilon_0 \frac{S}{x_{gl}}, \quad (3)$$

$$E_{int} = \frac{x_{gl} e_0 n_{e-h} (G-1)}{\epsilon \epsilon_0}, \quad (4)$$

where  $x_{gl}$  is the effective gain layer depth, not necessarily equal to the one defined by the implantation depth,  $S$  surface of the gain

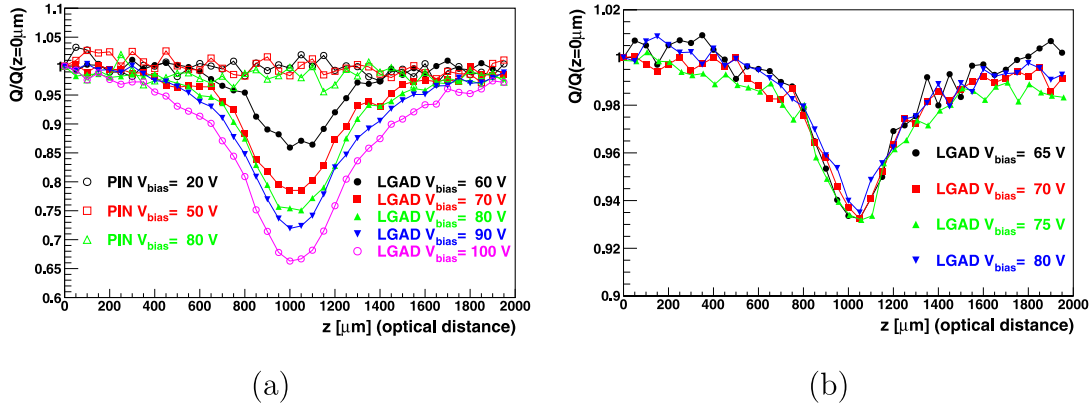


Fig. 6. (a) Relative change of collected charge with the beam spot size at different bias voltages for (a) HPK-PIN and HPK-T3.2 at 13 ke and (b) HPK-T3.1 at 77 ke. The collected charge was normalized to the one measured at  $z = 0$  (FWHM  $\approx 100 \mu\text{m}$ ).

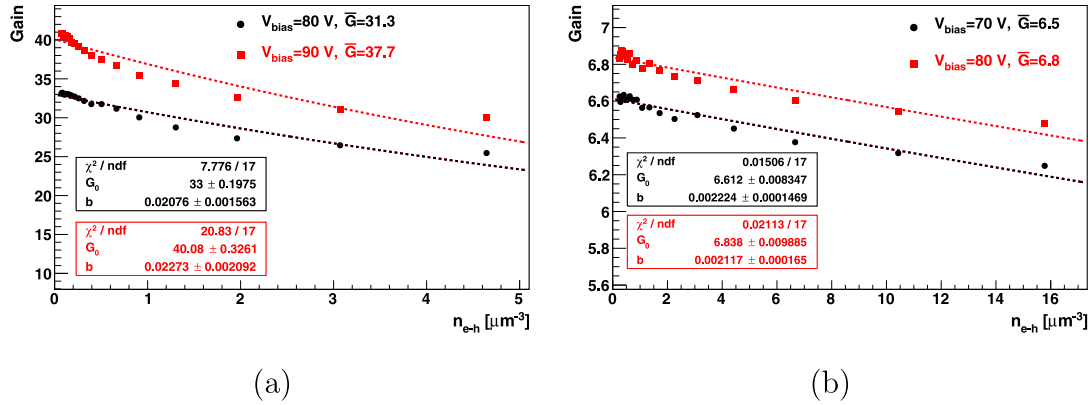


Fig. 7. Gain dependence on the concentration of the generated free carriers for (a) HPK-T3.2 sensor at  $Q_{gen} = 13 \text{ ke}$  (b) HPK-T3.1 sensor at  $Q_{gen} = 77 \text{ ke}$ . The dashed line is fit of the Eq. (7) to the data.

layer,  $Q_{gl}$  polarization charge,  $C_{gl}$  capacitance of the gain layer and  $\epsilon\epsilon_0$  permittivity of Silicon. The model makes no distinction about the design of the gain layer and all the design specifics are absorbed in the effective  $x_{gl}$ .

The model can be tested using the gain dependence on  $n_{e-h}$  shown in Figs. 7. The density of carriers was varied by beam spot width as described by Eq. (2). In the simplest approximation the gain depends on the average field in the gain layer and its thickness,

$$G = \frac{Q_{IR}}{Q_{gen}} \approx e^{\alpha_n(G, E, n_{e-h}) x_{gl}}, \quad (5)$$

where  $\alpha_n$  denotes the impact ionization coefficient at a given average electric field in the gain layer  $E$ . The impact ionization of holes ( $\alpha_p$ ) is much smaller at fields in the LGADs [13] and was not considered. If standard Chynoweth parametrization [14] is used and  $E_{int}$  is small in comparison with the external field given by applied bias voltage it can be written by using Taylor series expansion as

$$\alpha_n = a_0 e^{-\frac{E_c}{E - E_{int}}}, \quad \alpha_n \approx a_0 e^{-\frac{E_c}{E}} \left[ 1 - \frac{E_c}{E^2} E_{int} + \dots \right], \quad (6)$$

where  $E_c$  denotes the so called critical field and  $a_0$  is a prefactor. By insertion of Eqs. (4) and (6) in Eq. (5) the dependence of gain on free carrier density is obtained

$$G \approx G_0^{1-b} n_{e-h}, \quad b = \frac{E_c}{E^2} \frac{x_{gl} e_0 (\bar{G} - 1)}{\epsilon\epsilon_0}. \quad (7)$$

Strictly, parameter  $b$  depends on  $G$  which complicates the solution of Eq. (7), but in the investigated range the gain variation is much

smaller than that of the  $n_{e-h}$ , hence an average gain  $\bar{G}$  can be used. The fits of Eq. (7) are shown in Figs. 7a,b for two different voltages. The assumptions made in the model can be checked by extraction of  $x_{gl}$  from the fit parameters. If one assumes that the average field in the gain layer is in the first approximation given by  $V_{gl}/x_{gl}$  (neglecting small correction  $(V_{bias} - V_{fd})/D$  for  $V_{bias} > V_{fd}$ ) a rough estimation of  $x_{gl}$  can be extracted from  $b$  as

$$x_{gl} \approx \sqrt[3]{\frac{b V_{gl}^2 \epsilon\epsilon_0}{E_c e_0 (\bar{G} - 1)}}. \quad (8)$$

Using  $E_c = 203 \text{ V}/\mu\text{m}$  [13], and  $b, \bar{G}$  as determined from the measurements,  $x_{gl} \sim 1.85 \mu\text{m}$  for T3.2 and  $x_{gl} \sim 1.2 \mu\text{m}$  for T3.1 were obtained which roughly agree with the design values and therefore confirm the validity of the assumptions.

The same gain can be achieved for two different bias voltages if there is large enough difference in the density of carriers,  $G(V_{bias,1}, n_{e-h,1}) = G(V_{bias,2}, n_{e-h,2})$ . In such case  $\Delta E_{int}$  due to  $\Delta n_{e-h}$  (see Eq. (4)) is compensated by the external field due to different applied bias voltage  $\Delta V_{bias} = V_{bias,1} - V_{bias,2}$ ,

$$\frac{x_{gl} e_0 \Delta n_{e-h} (G - 1)}{\epsilon\epsilon_0} = \frac{\Delta V_{bias}}{D}, \quad V_{bias,1}, V_{bias,2} > V_{fd}. \quad (9)$$

The left and right side of Eq. (9) can be independently evaluated and compared, for the gain and density of carriers indicated in Fig. 7a. At  $G(80 \text{ V}, 0.5 \mu\text{m}^{-3}) = G(90 \text{ V}, 3 \mu\text{m}^{-3}) = 32$  for the HPK-T3.2. The left side evaluates to  $\Delta E_{int} = 0.22 \text{ V}/\mu\text{m}$  and the right  $\Delta V_{bias}/D = 0.2 \text{ V}/\mu\text{m}$ , which are in very good agreement considering the assumptions made.

The same calculations were also done at lower laser intensity (smaller  $n_{e-h}$ ) and higher gain for sample HPK-T3.1 (e.g. for  $G(70\text{ V}, 2\ \mu\text{m}^{-3}) = G(80\text{ V}, 16\ \mu\text{m}^{-3}) = 6.8$ ,  $\Delta E_{int} = 0.17\text{ V}/\mu\text{m}$  shown in Fig. 7b), all agreeing reasonably well.

#### 4. Discussion

Eq. (4) explains the properties of LGAD operation for heavily ionizing particles. Their ionization density can exceed the one from m.i.p. for up to several orders of magnitude depending on the energy and charge. High ionization density therefore reduces the gain to the level where balance between external and screening field can be maintained. This is clearly shown in Ref. [7].

Even for minimum ionizing particles the screening of the field can be significant with respect to low intensity laser pulse as shown for  $^{90}\text{Sr}$  in Fig. 4a. The density of ionization of  $^{90}\text{Sr}$  ( $n_{e-h,^{90}\text{Sr}}$ ) can be estimated from the  $G(120\text{ V}, n_{e-h,^{90}\text{Sr}}) = G(90\text{ V}, \approx 0) = 30$ ;  $n_{e-h,^{90}\text{Sr}} \approx 7.5\ \mu\text{m}^{-3}$  can be thus extracted from Eq. (7). Assuming that the most probable generated charge is  $\sim 3200\ e_0$  the required ionization radius is around  $1.6\ \mu\text{m}$ , which is a reasonable value for low energy electrons.

The screening model can also qualitatively explain the unexpected observation that the gain of the LGAD for highly ionizing particles reaches its maximum at  $V_{fd}$  and then decreases with bias voltage [6,7]. The widening of the drifting charge cloud due to diffusion effectively reduces the screening and the reduced effect of diffusion at higher bias voltages can have a larger adverse effect than the increase of external bias. Similar conclusions apply to the tracks crossing the detector at an angle, where less screening and higher gain can be achieved [8].

Eq. (7) favors a slightly shallower gain layer design i.e. small  $x_{gl}$  for highly ionizing particles (smaller  $b$ ). This also explains the difference between HPK-T3.1 and HPK-T3.2 sensors observed in Figs. 5c,d where larger dependence of gain on ionization density is observed for HPK-T3.2 at roughly the same gain.

#### 5. Conclusions

The suppression of the gain for heavily ionizing particles and minimum ionizing particles crossing LGADs at an angle were investigated with infra-red transient current technique, where laser intensity and beam spot were used to modify the ionization density in the detector. A clear dependence of gain on ionization density was observed. A simple model assuming polarization of the gain layer due to multiplication was proposed. The model successfully explained the measurements for two different gain layer designs. Its predictions show a large decrease of gain for heavily ionizing particles.

#### Declaration of competing interest

The authors declare that they have no known competing financial interests or personal relationships that could have appeared to influence the work reported in this paper.

#### Data availability

Data will be made available on request.

#### Acknowledgment

The authors acknowledge the financial support from the Slovenian Research Agency (ARRS J1-1699, ARRS P1-0135).

#### References

- [1] G. Pellegrini, et al., Technology developments and first measurements of Low Gain Avalanche Detectors (LGAD) for high energy physics applications, Nucl. Instr. Meth. A 765 (2014) 12.
- [2] H.F.-W. Sadrozinski, A. Seiden, N. Cartiglia, 4D tracking with ultra-fast silicon detectors, Rep. Prog. Phys. 81 (2) (2018) 026101.
- [3] A. Vignati, et al., Innovative thin silicon detectors for monitoring of therapeutic proton beams: Preliminary beam tests, JINST 12 (2017).
- [4] F.U. Pur, et al., Feasibility study of a proton CT system based on 4D-tracking and residual energy determination via time-of-flight, Phys. Med. Biol. C12056 (2022) 095005.
- [5] M. Andra, Development of low-energy X-ray detectors using LGAD sensors, J. Synchrotron Radiat. 26 (4) (2019) 1226.
- [6] M.C. Jimenz Ramos, et al., Study of ionization charge density-induced gain suppression in LGADs, Sensors 22 (2022) 1080.
- [7] M. Jakšić, et al., Ion microbeam studies of charge transport in semiconductor radiation detectors with three-dimensional structures: An example of LGAD, Front. Phys. 10 (2022) 877577.
- [8] E. Carras, M. Fernandez, M. Moll, Gain reduction mechanism observed in Low Gain Avalanche Diodes, Nucl. Instr. Meth. A 1031 (2022) 166530.
- [9] G. Kramberger, Advanced transient current technique systems, PoS (Vertex2014) 032.
- [10] S. Ritt, Design and performance of the 6 GHz waveform digitizing chip DRS4, in: 2008 IEEE Nuclear Science Symposium Conference Record, 14835524, <http://dx.doi.org/10.1109/NSSMIC.2008.4774700>.
- [11] K.N. Yu, et al., Comparison among alpha-particle energy losses in air obtained from data of SRIM, ICRU and experiments, Appl. Radiat. Isotopes 59 (2003) 363–366.
- [12] A. Howard, et al., LGAD measurements from different producers, in: Presented At 37th RD50 Workshop, Zagreb, 2020.
- [13] R. Van Oversaeten, H. De Man, Measurement of the ionization rates in diffused silicon p-n junctions, Solid-State Electron. 13 (1970) 583–608.
- [14] A.G. Chynoweth, Ionization rates for electrons and holes in silicon, Phys. 346 Rev. 109 (5) (1958) 1537.